Lateral resistance of pipes and strip anchors buried in dense sand

Kshama Roy[1], Bipul Hawlader[2*], Shawn Kenny[3] and Ian Moore[4]

[1]Pipeline Stress Specialist, Northern Crescent Inc., 816 7 Ave SW, Calgary, Alberta T2P 1A1, Canada; formerly PhD Candidate, Department of Civil Engineering, Faculty of Engineering and Applied Science, Memorial University of Newfoundland, St. John's, Newfoundland and Labrador A1B 3X5, Canada

[2]**Corresponding Author:** Professor and Research Chair in Seafloor Mechanics, Department of Civil Engineering, Faculty of Engineering and Applied Science**,** Memorial University of Newfoundland, St. John's, Newfoundland and Labrador A1B 3X5, Canada
Tel: +1 (709) 864-8945 Fax: +1 (709) 864-4042 E-mail: bipul@mun.ca

[3]Associate Professor, Department of Civil and Environmental Engineering, Faculty of Engineering and Design, Carleton University, 1125 Colonel By Drive, Ottawa, ON, K1S 5B6

[4]Professor and Canada Research Chair in Infrastructure Engineering, GeoEngineering Centre at Queen's – RMC, Queen's University, Kingston, ON, K7L 4V1

Number of Figures: 8

Number of table: 2

KEYWORDS: pipeline and anchor, Mohr-Coulomb model, dense sand, lateral loading, pipe−soil interaction

Abstract

The response of buried pipes and vertical strip anchors in dense sand under lateral loading is compared based on finite-element (FE) modeling. Incorporating strain-softening behaviour of dense sand, the progressive development of shear bands and the mobilization of friction and dilation angles along the shear bands are examined, which can explain the variation of peak and post-peak resistances for anchors and pipes. The normalized peak resistance increases with embedment ratio and remains almost constant at large burial depths. When the height of an anchor is equal to the diameter of the pipe, the anchor gives approximately 10% higher peak resistance than that of the pipe. The transition from the shallow to deep failure mechanisms occurs at a larger embedment ratio for anchors than pipes. A simplified method is proposed to estimate the lateral resistance at the peak and also after softening at large displacements.

Introduction

Buried pipelines are one of the most efficient modes of transportation of hydrocarbons, both in onshore and offshore environments. Permanent ground deformations caused by various factors (e.g. landslides, slow movement of soil in a slope, nearby excavation) and thermal expansion (e.g. lateral displacement of the pipeline at the side bends) result in relative displacement between the pipe and surrounding soil. To develop the force–displacement relationships, in addition to the research on buried pipelines, studies on strip anchors (simply referred to as “anchor” in this paper) have been utilized, assuming that a geometrically similar pipe and anchor essentially behave in a similar fashion (Dickin 1994; Ng 1994). However, comparing the behaviour of buried pipes and anchors, some contradictory results have been obtained. Based on centrifuge tests, Dickin (1994) showed no significant difference between uplift behaviour of pipes and anchors. Reanalyzing 61 tests on model pipes and 54 on anchors, White et al. (2008) showed that the same limit equilibrium

(LE) method overpredicts the maximum uplift resistance (mean value) of pipes by 11%, while it underpredicts the anchor resistance by 14%. The authors suggested that this discrepancy might result simply from the feature of the database or be an indication that pipes and anchors behave differently.

Very limited research comparing lateral resistance of pipes and anchors is available. In a limited number of centrifuge tests, Dickin (1988) showed no significant difference between the force–displacement curves for pipes and anchors up to the peak resistance; however, the anchors give higher resistance than pipes after the peak.

Pipelines and anchors buried in dense sand are the focus of the present study. Anchors can be installed directly in dense sand (Das and Shukla 2013). Buried pipelines are generally installed into a trench. When the trench is backfilled with sand, the backfill material might be in a loose to medium dense state. However, during the lifetime of an onshore pipeline, the backfill sand might be densified due to traffic loads, nearby machine vibrations or seismic wave propagation (Kouretzis et al. 2013). Furthermore, Clukey et al. (2005) showed that the relative density of sandy backfill of an offshore pipe section increased from less than ~ 57% to ~ 85–90% in 5 months after construction, which has been attributed to wave action at the test site in the Gulf of Mexico. The behaviour of buried pipes and anchors can be compared through physical modeling and numerical analysis. Physical modeling is generally expensive, especially the full-scale tests at large burial depths, in addition to having some inherent difficulties, including the examination of the progressive formation of thin shear bands in dense sand. Through a joint research project between Memorial University of Newfoundland and Queen's University, Canada, the authors and their co-workers used the particle image velocimetry (PIV) technique (White et al. 2003) in full-scale tests for lateral pipe–soil interaction in both loose and dense sand (Burnett 2015). While PIV results provide deformation of the soil particles and location of the shear bands, tests on a wide range of burial depths could not be conducted. In addition, a number of centrifuge tests were also conducted using the geotechnical centrifuge at C-CORE (Daiyan et al. 2011; Debnath 2016).

Force–displacement behaviour is generally expressed in normalized form using $N_h = F_h/(\gamma HD)$ and $\tilde{u} = u/D$, where D is the diameter of the pipe (replace D with height of the anchor (B) for anchor–soil interaction), γ is the unit weight of the soil, F_h is the lateral force per unit length of the pipe/anchor, H is the depth of the center of the pipe or anchor and u is the lateral displacement. The burial depth is also expressed in normalized form using the "embedment ratio, $\widetilde{H} = H/D$."

A considerable number of physical experiments were conducted on lateral pipe–soil interaction (Trautmann 1983; Hsu 1993; Daiyan et al. 2011; Burnett 2015; Monroy et al. 2015). Guo and Stolle (2005) compiled data from 11 experimental tests on dense sand and showed that the maximum dimensionless force (N_{hp}) increases with $\widetilde{H}$ and decreases with an increase in pipe diameter. Note, however, that a very limited number of tests for large diameters at large $\widetilde{H}$ are available. Most of the tests for $\widetilde{H} > 7$ were conducted using small diameter pipes (D = 25–50 mm), except for the Trautmann (1983) tests with a 102-mm diameter pipe. Physical experiments on dense sand show a reduction of resistance after the peak (Trautmann 1983).

Lateral pipeline–soil interactions can occur in the field in two ways: (i) soil can push the pipeline when ground moves (e.g., during landslides), and (ii) the pipeline can push the soil—for example, thermal expansion due to operating temperature increase could cause lateral displacement at horizontal bends. When the N_h–$\tilde{u}$ relation is used to model the force on the pipe due to ground movement, the use of the maximum dimensionless force (N_{hp}) is conservative because it gives a higher force on the pipe. However, for the latter cases, a lower bound estimation of soil resistance is necessary for safe design (Oswell 2016). For example, Oswell (2016) suggested that the consideration of a higher soil resistance is often non-conservative when a pipeline pushes the soil due to thermal expansion at the side bends. In these cases, softer horizontal soil springs considering the post-peak N_h would be conservative because it will give greater pipe displacement and bending stress. In the current industry practice, stresses in the pipeline are calculated based on both upper and lower bound soil resistances, and the calculated stresses for the maximum operating temperature should not exceed the allowable values defined in the design code. The lateral displacements at the bend, when the stresses in the pipe exceeds the acceptable limits, could be higher than the displacement required to mobilize the peak force, especially when the soil has strain-softening behaviour (e.g., dense sand). In such cases, consideration of post-peak degradation of soil resistance will improve the modelling of structural response.

The existing design guidelines recommend simplified methods to calculate N_{hp} based on angle of internal friction of the soil, ϕ' (ALA 2005). However, as will be discussed in the following sections, N_{hp} depends on mobilized shear resistance of soil along the slip planes that form due to relative displacement between the pipe and surrounding soil.

Similar to pipeline research, a large number of experimental studies have been conducted on lateral anchor–soil interaction for loose to dense sands, with a main focus on the maximum capacity, N_{hp} (Neely et al. 1973; Das et al. 1977; Akinmusuru 1978; Dickin and Leung 1983; Hoshiya and Mandal 1984; Choudhary and Das 2017). Among the experimental studies, limited number of tests were conducted on dense sands (e.g. Dickin and Leung 1983). However, theoretical studies (Neely et al 1973; Dickin and Leung 1985; Murray and Geddes 1989), finite-element analyses (Rowe and Davis 1982; Dickin and King 1993) and finite-element limit analyses (Merifield and Sloan 2006; Kumar and Sahoo 2012; Bhattacharya and Kumar, 2013) have been performed to calculate the peak lateral resistance assuming a constant representative value of friction angle (ϕ') for dense sand. Similar to pipes, physical experiments show a post-peak degradation of lateral resistance for anchors in dense sand (Dickin and Leung 1983). The use of a resistance after post-peak reduction might be safe for anchors buried in dense sand as the anchor might undergo considerably large displacements. Furthermore, some studies suggested that the modeling of progressive development of shear bands would better simulate the response of anchors in dense sand (e.g. Tagaya et al. 1983; Sakai and Tanaka 2007).

The lateral resistance evolves from a complex deformation mechanism and the stress–strain behaviour of soil around the pipe and anchor. More specifically, the progressive development of shear bands in dense sand due to strain-softening and mobilization of shear resistance along these planes govern the lateral resistance. The stress–strain behaviour of dense sand involves the pre-peak hardening, post-peak softening, relative density and effective mean stress (p') dependent ϕ' and ψ. Therefore, single representative values of ϕ' and/or ψ for the Mohr-Coulomb model in FE simulation or in simplified limit equilibrium analysis should be carefully selected. For anchors, Dickin and Leung (1983) showed that the peak friction angle gives considerably higher resistance compared to the experimental results. Similarly, for pipelines in dense sand, O'Rourke and Liu (2012) showed that ALA (2005) or PRCI (2004) guidelines that adopted Hansen's (1961) study on piles give N_{hp} more than twice of Trautmann and O'Rourke's (1983) recommendations based on physical modeling.

The aim of the present study is to conduct FE analyses to identify potential reasons behind the similarities and differences between the response of pipes and anchors in dense sand subjected to lateral loading. The progressive formation of shear bands with lateral displacement is simulated implementing a modified form of the Mohr–Coulomb model for dense sand. The mobilization of ϕ' and ψ along the shear band is examined to explain soil failure mechanisms and mobilized resistances at the peak and post-peak degradation stages. Finally, a set of simplified equations is proposed for practical applications.

Problem statement and finite-element modeling

An anchor or a section of pipe is placed at the desired embedment ratio ($\widetilde{H}$) in dense sand and then pulled laterally. Two-dimensional FE analyses in plane strain condition are performed using Abaqus/Explicit FE software (Dassault Systèmes 2010). Figure 1 shows the typical FE mesh at the start of lateral loading. Four-node bilinear plane-strain quadrilateral elements (CPE4R in Abaqus) are used for modeling the soil while the pipe/anchor is modelled as a rigid body. The thickness of the anchor is 200 mm. Analyses are also performed for other thicknesses (100–300 mm); however, no significant effects on lateral resistance are found. The bottom of the FE domain is restrained from any horizontal and vertical movement, while all the vertical faces are restrained from lateral movement. The boundaries are placed at a sufficiently large distance from the pipe/anchor to minimize boundary effects on lateral resistance. To avoid numerical issues related to large mesh distortion, soil is defined as an adaptive mesh domain with the default Lagrangian type boundary regions (lines in the present two-dimensional analysis), which creates new smooth mesh with improved aspect ratios at given intervals.

The interface behaviour is modeled using a surface-based contact method that allows slip and separation between pipe/anchor and soil. The frictional resistance is defined using the interface friction coefficient (μ) as $\mu = \tan(\phi_\mu)$, where ϕ_μ is the interface friction angle. ϕ_μ depends on interface characteristics and relative movement between the pipe/anchor and soil and typically lies between 50 and 100% of the peak friction angle (Yimsiri et al. 2004). Such variation of ϕ_μ can change the maximum lateral resistance by 5%–8% (Yimsiri et al. 2004; Jung et al. 2013). In the present study, $\phi_\mu = 17.5°$ is used.

The numerical analysis is conducted in two steps. In the geostatic step, all the soil elements are brought to the in-situ stress condition under K_0 = 1.0, where K_0 is the at-rest earth pressure coefficient. The value of K_0 does not significantly affect the lateral resistance in FE analysis (Jung et al. 2016). In the second step, the pipe/anchor is displaced laterally by specifying a displacement boundary condition at the reference point (center of the pipe/anchor).

Modeling of soil

Two soil models are used in this study: (i) Mohr–Coulomb (MC) and (ii) a modified Mohr–Coulomb (MMC) model. In the MC model, the angles of internal friction (ϕ') and dilation (ψ) are given as input, which remain constant during FE analysis. However, in the MMC model, the mobilized ϕ' and ψ are updated during the progress of FE analysis, as a function of accumulated plastic shear strain (γ^p) and mean effective stress (p'). Note that modified forms of the MC model have also been used in previous studies (Guo and Stolle 2005; Jung et al. 2013; Robert and Thusyanthan 2014). The details of the MMC model used in the present study have been presented by the authors elsewhere (Roy et al. 2016). The key features of the MMC model are presented below, while the mathematical equations are listed in Table 1 (Eqs. (1)–(10)).

i) Laboratory tests on dense sand show that ϕ' and ψ vary with D_r, γ^p, p' and mode of shearing (triaxial (TX) or plane strain (PS)). However, constant representative values of ϕ' and ψ are commonly used in the MC model. The peak friction angle (ϕ'_p) increases with D_r but decreases with p' (Bolton 1986; Houlsby 1991), which are modeled using Eqs. (1) to (3) as in the work of Bolton (1986), where ϕ'_c is the critical state friction angle and A_ψ and k_ψ are two constants. Bolton (1986) suggested A_ψ = 5.0 and 3.0 for plane strain and triaxial conditions, respectively. Chakraborty and Salgado (2010) recommended A_ψ = 3.8 for both TX and PS conditions from their analysis of test results on Toyoura sand. In the present study, $A_\psi = 5$ with $\phi'_p - \phi'_c \leq 20°$ for PS configuration is used (Bolton 1986).

ii) The mobilization of ϕ' and ψ with γ^p is modeled using Eqs. (6) to (9), which show that ϕ' and ψ gradually increase from the initial value $(\phi'_{in}, 0)$ to the peak (ϕ'_p, ψ_p) at γ^p_p. In the post-peak region, ϕ' and ψ are reduced exponentially, as in Eqs. (7) and (8), from the peak to the critical state values $(\phi' = \phi'_c, \psi = 0)$ at large γ^p. As the analysis is performed for the PS condition, ϕ'_c =35° is used, which is typically 3°–5° higher than that of the TX configuration (Bishop 1961; Cornforth 1964; Pradhan et al. 1988; Yoshimine 2005).

iii) The Young's modulus (E) is calculated using Eq. (10) (Janbu 1963; Hardin and Black 1966), where p' is the initial mean effective stress at the springline of the pipe, p'_a is the atmospheric pressure (= 100 kPa), K is a material constant, and n is an exponent. Equation (10) has also been used in the previous studies for FE modeling of pipe–soil interaction (Yimsiri et al. 2004; Guo and Stolle 2005; Daiyan et al. 2011; Jung et al. 2013). In the present study, K = 150 and n = 0.5 is used. The Poisson's ratio of 0.2 is used for the soil, which is considered as the representative value for dense sand (Jefferies and Been 2006).

The implementation of the MMC model in Abaqus using a user defined subroutine has been discussed elsewhere (Roy et al. 2016).

Model tests simulations

In order to show the performance of the present FE modeling, simulations are first performed for two 1g model tests with 100-mm diameter pipe and two centrifuge tests with 1,000-mm high strip anchor (in prototype scale), conducted by Trautmann (1983) and Dickin and Leung (1983), respectively. These tests were conducted in dense sand having $D_r \sim 80\%$. Dickin and Leung (1983) conducted tests on a fine and fairly uniform dense dry Erith sand ($\gamma \sim 16$ (kN/m^3)). A comprehensive experimental study, including plane strain and triaxial compression tests, on this sand shows that ϕ'_p increases with reduction of confining pressure, and ϕ'_p is higher in PS condition than in TX condition (Eqs. (1)–(3)). Dickin and Laman (2007) simulated the response of anchors in this sand at loose condition using a friction angle of 35°, which is similar to ϕ'_c (Dickin 1994). Trautmann (1983) conducted the tests on clean and subangular dense Cornell filter sand (γ = 17.7 (kN/m^3). Analyzing a large number of tests on different sands, Bolton (1986) suggested Q = 10 and R = 1 for Eq. (1), and A_ψ = 5 and k_ψ = 0.8 for Eqs. (2) and (3), respectively, for PS condition. Roy et al. (2016) calibrated the present MMC model against laboratory test results on Cornell filter sands and obtained the values of C_1, C_2 and m to model mobilized ϕ' and ψ with γ^p (Eqs. (4)–(9)). Dickin and Leung (1983) did not provide the stress–strain curves of Erith sand used in their centrifuge modeling; therefore, the values of C_1, C_2 and m of this sand are assumed to be the same as Cornell filter sand.

FE simulations are performed for $\widetilde{H}$ = 1.5 and 5.5 for pipes and $\widetilde{H}$ = 1.5 and 4.5 for anchors, to explain the effects of the embedment ratio. The soil parameters used in FE simulations are listed in Table 2. Although c' = 0 for sand, a small value of c'(≤ 0.01 kPa) is used to avoid numerical issues. Further details on lateral pipe–soil interaction and performance of the MMC model can be found in Roy et al. (2016).

Force–displacement behaviour of anchor

Figure 2 (a) shows the normalized force–displacement curves for anchors. The FE simulation with the MMC model for $\widetilde{H}$ = 1.5 shows that N_h increases with $\tilde{u}$, reaches the peak (N_{hp}) at $\tilde{u}$ ~ 0.05 (point A) and then quickly decreases to point B, which is primarily due to the strain-softening behaviour of dense sand. After that, N_h remains almost constant. In the present study, the rapid reduction of the lateral resistance segment of the N_h–$\tilde{u}$ curve (e.g. segment AB for $\widetilde{H}$ = 1.5) is called the "softening segment," while the segment after softening (e.g. segment after point B) is the "large-deformation segment." Although some cases show a slight decrease in resistance in the large deformation segment, the resistance at the end of softening segment (e.g. at point B) is considered to be the "residual resistance (N_{hr})."

For comparison, centrifuge test results from Dickin and Leung (1983) are also plotted in Fig. 2(a). The following are the key observations: (i) N_{hp} and N_{hr} obtained from FE analysis with the MMC model are comparable to those obtained from the centrifuge tests; (ii) both centrifuge and FE simulations with the MMC model have softening and large-deformation segments in the N_h–$\tilde{u}$ curve; (iii) $\tilde{u}$ required to mobilize a N_h (e.g. N_{hp} and N_{hr}) is significantly higher in centrifuge tests than in FE simulations. Regarding this discrepancy, it is to be noted that, conducting 1g and centrifuge tests for uplift resistance in dense sand, Palmer et al. (2003) showed that while the peak resistances obtained from these tests are comparable, the normalized mobilization distance in the centrifuge is significantly higher than that required in 1g tests. They also inferred that the centrifuge scaling law may not be fully applicable to strain localization and shear band formation in dense sand, although the magnitude of resistance could be successfully modeled. The present FE analysis for lateral anchor–soil interaction also shows a similar trend, which implies that the mobilization distance in FE analysis might be comparable to 1g tests.

A very similar trend is found for $\widetilde{H}$ = 4.5 when the centrifuge test results are compared with FE simulation using the MMC model. However, in this case, N_{hr} and the large-deformation segment of the N_h–$\tilde{u}$ curve could not be identified from centrifuge test results because the test was stopped at $\tilde{u}$ = 0.4, before the completion of softening. FE calculated N_{hp} and N_{hr} for $\widetilde{H}$ = 4.5 are higher than those values for $\widetilde{H}$ = 1.5.

<u>Force–displacement behaviour of pipe</u>

Figure 2(b) shows that the force–displacement curves obtained from FE analysis with the MMC model are very similar to the model test results of Trautmann (1983). For a high $\tilde{H}$ (= 5.5), there is a post-peak reduction of N_h; however, for a low $\tilde{H}$ (= 1.5), no significant post-peak reduction of N_h is found. Unlike Fig. 2(a), no significant discrepancy in the normalized mobilization distance between the model test and FE simulation results is found, because in this case the tests were conducted at 1g while the tests presented in Fig. 2(a) were conducted at 40g.

The model tests conducted by Audibert and Nyman (1978) using a 25-mm diameter pipe buried in dense Carver sand also show similar response: no significant post-peak degradation of N_h for shallow-buried pipelines ($\tilde{H}$ = 1.5 and 3.5), but a considerable post-peak degradation for deeper pipelines ($\tilde{H}$ = 6.5 and 12.5).

As will be discussed later in the "Failure mechanisms" section that the shear bands form gradually with lateral displacement of the pipe/anchor, and plastic shear strains generate in the shear band even before the mobilization of peak resistance. Therefore, the shape of pre-peak N_h–$\tilde{u}$ curves in Fig. 2 is influenced by: (i) burial depth (i.e. p') dependent Young's modulus, E (Eq. (10)), (ii) p' and γ^p dependent ϕ' and ψ (Eqs. (6)–(9)), and (iii) burial depth dependent shape of the slip planes, as will be shown later in Fig. 7. Proper estimation of E is a challenging task. Based on multiple linear regression analyses of data, O'Rourke (2010) proposed an empirical equation for E as a function of vertical effective stress at pipe centre and dry unit weight of soil. Jung et al. (2013) used a strain-compatible secant modulus for modeling elastic behaviour, which was derived based on the hyperbolic stress–strain relationship of Duncan and Chang (1970), and showed a good match between the force–displacement curves obtained from numerical simulation and model test results. The slight difference in N_h–$\tilde{u}$ curves between model test and the present FE simulation results, as shown in Fig. 2(b), could be reduced further by selecting a more appropriate value for Young's modulus.

Limitations of the Mohr-Coulomb model

To show the advantages of the MMC model, three FE simulations with the MC model are performed for $\widetilde{H}$ = 1.5 using three sets of ϕ' and ψ values (ϕ' = 50°,ψ = 19°; ϕ' = 44°,ψ = 16° and ϕ' = 35°,ψ = 0°). Here, for a given ϕ', the value of ψ is calculated using Eq. (3) in Table 1. As expected, for the MC model, N_h increases with $\tilde{u}$, reaches the peak (N_{hp}) and then remains constant (Fig. 2(a)). Figure 2(a) also shows that the MC model for ϕ'=44° and ψ=16° gives N_{hp} comparable to the peak of the centrifuge test results. For ϕ'=50° and ψ=19°, N_{hp} is significantly higher, and for ϕ'=35° and ψ=0°, N_{hp} is significantly lower than the centrifuge test results. Although it is not explicitly mentioned in the design guidelines, equivalent (representative) values for these two parameters should be carefully selected, as they vary with γ^p (Roy et al. 2016). In general, the equivalent values of ϕ' and ψ should be smaller than the peak and higher than the critical state values. For example, Dickin and Leung (1983) mentioned that if the peak friction angle obtained from laboratory tests is used, the theoretical models (Ovesen and Stromann 1972; Neely et al. 1973) significantly overestimate the resistance as compared to model test results. Therefore, although ϕ'_p > 50° was obtained from laboratory tests, they used an equivalent friction angle of 39.4°–43.5° to calculate N_{hp}. Another key observation from Fig. 2(a) is that the simulations with the MC model do not show any post-peak degradation of N_h, as observed in centrifuge tests.

The difference between the N_h–$\tilde{u}$ curves with the MC and MMC models can be further explained from the progressive development of shear bands, the zones of localized plastic shear strain, $\gamma^p = \int_0^t \sqrt{\frac{3}{2}\left(\dot{\epsilon}^p_{ij}\dot{\epsilon}^p_{ij}dt\right)}$, where $\dot{\epsilon}^p_{ij}$ is the plastic deviatoric strain rate tensor (Figs. 3(a–d)).

These figures show the variations of γ^P at points C, D, E and F in Fig. 2(a). Three distinct shear bands (f_1–f_3) form in all the cases. However, the approximate angle of the shear band f_1 to the vertical increases with ϕ' and ψ, as shown by drawing lines through the shear bands (Fig. 3(e)), which in turn increases the size of the passive failure wedge and thereby lateral resistance. An opposite trend, a decrease in size of the active failure wedge (on the left side of the anchor) with an increase in ϕ' and ψ is found; however, the active zone does not have a significant effect on lateral resistance. Further details on soil failure mechanisms, including the comparison with physical model test results, are available in Roy et al. (2016, 2016a).

Mesh sensitivity

As the MMC model considers the strain-softening behaviour of dense sand, FE simulations with this model are expected to be mesh sensitive. More specifically, the formation of shear bands and mobilization of ϕ' and ψ need to be modeled properly. For sand, the ratio between the thickness of the shear band (t_s) and the mean particle size (d_{50}) varies between 3 and 25; the lower values mostly correspond to coarse-grained sands (Loukidis and Salgado 2008; Guo 2012). As the soil is modeled as a continuum in the FE analysis, the width of the shear band can be controlled by varying element size, which is described by the characteristic length of the finite element (t_{FE}). Very small t_{FE} gives an unrealistically thin shear band, while large t_{FE} cannot capture strain localization properly. The ratio of t_s/t_{FE} also depends on loading conditions. For example, Loukidis and Salgado (2008) used $t_{FE} = t_s$ in the zone of strain localization near the pile to calculate the shaft resistance in dense sand. However, the deformed mesh under the footing in dense sand shows $t_s \sim (2–3)t_{FE}$ (Tejchman and Herle 1999; Tejchman and Górski 2008), which is consistent with model tests results (Tatsuoka et al. 1991). As will be shown later, during lateral movement of the pipe, strain localization extends to more than one element. Therefore, $t_{FE} < t_s$ should be used to capture the strain localization properly. Assuming $d_{50} \sim 0.5$ mm and $t_s/d_{50} \sim 25$ for fine sand, $t_s \sim 12.5$ mm is calculated, which is also consistent with experimentally observed shear band width. For example, Sakai et al. (1998) showed $t_s \sim 9$ mm for fine Soma sand and Uesugi et al. (1988) found $t_s \sim 8$ mm for Seto sand.

Several authors proposed element scaling rules to reduce the effects of FE mesh on simulated results (Pietruszczak and Mróz 1981; Moore and Rowe 1990; Andresen and Jostad 2004; Anastasopoulos et al. 2007). Using the work of Anastasopoulos et al. (2007) and assuming the reference FE mesh $t_{FE\_ref} = 10$ mm, analyses are performed for $t_{FE} = 30$ mm and 50 mm, where γ_c^p in Eq. (4) is scaled by a factor of $f_{scale} = (t_{FE\_ref}/t_{FE})^m$, where m is a constant. Anastasopoulos et al. (2007) suggested $m = 1$ (i.e. f_{scale} is inversely proportional to element size) for fault rupture propagation. However, a number of FE simulations of lateral loading of pipes for varying geotechnical properties, element size, and pipe diameter show that $m \sim 0.7$ gives a better f_{scale} than $m = 1$ for mesh independent N_h–$\tilde{u}$ curves. As an example, for $D_R = 80\%$, $\gamma_c^p = 0.132$ for both 50-mm and 10-mm mesh, when the scaling rule is not used. However, $\gamma_c^p = 0.132*(10/50)^{0.7} = 0.043$ for 50-mm and $\gamma_c^p = 0.132$ for 10-mm mesh when the scaling rule is used.

Figure 4 shows the sample mesh sensitivity analysis results for a 500-mm diameter pipe. If the scaling rule is not used, the peak resistance and the rate of post-peak degradation are considerably higher for coarse mesh ($t_{FE} = 50$ mm) than for fine mesh ($t_{FE} = 10$ mm). However, the mesh size effect on N_h is negligible at very large $\tilde{u}$, because at this stage the shear strength along the shear bands is simply governed by the critical state parameters. Figure 4 also shows that the scaling rule brings the N_h–$\tilde{u}$ curves closer for the three mesh sizes. A very similar trend is found for other diameters. In the present study, except for mesh sensitive analysis, $t_{FE} \sim 10$ mm, while a few rows of elements near the pipe have $t_{FE} < 10$ mm.

Peak anchor resistance

Figure 5 shows that the peak resistance obtained from FE analyses with the MMC model is higher for a 500-mm anchor than that of a 1,000-mm anchor. The normalized peak dimensionless force (N_{hp}) increases with $\widetilde{H}$; however, it remains almost constant at large embedment ratios. Physical model test results available in the literature are also included in this figure for comparison. A significant difference between N_{hp} for different anchor heights is also evident in the physical model tests; for example, compare the triangles and open squares in Fig. 5 that represent N_{hp} for 50-mm and 1,000-mm anchors, respectively. In other words, there is a "size effect" on N_{hp}, and that can be explained using the MMC model. The dependency of ϕ' and ψ on the mean effective stress (p') is the primary cause of size effect. For a larger anchor height, overall p' is higher, which gives smaller mobilized ϕ' and ψ (Eqs. (1)–(3)). The smaller values of ϕ' and ψ reduce not only the frictional resistance along the slip plane but also the inclination of the slip plane to the vertical and thereby the size of the passive failure wedge. Moreover, as discussed later in the "Failure mechanisms" section, once the failure wedges are formed, the inclination of a shear band (e.g. f_1 in Fig. 3(d)) does not change significantly with anchor displacement. This implies that the size effect also exists in residual resistance because the size of failure wedges governs by the p' dependent ϕ' and ψ at the early stage of displacements, not by the critical state values (independent of p'). Further discussion on this issue is provided later in the "Proposed simplified equations" section.

Comparison of response between pipes and strip anchors

Figure 6 shows the N_h–$\tilde{u}$ curves for a similar-sized pipe and anchor (B = D = 500 mm), on which the points of interest for further explanation are labeled (circles, squares and diamonds are for the peak, residual and large displacements, respectively). Similar to physical model test results for anchors and pipes (Dickin and Leung 1983; Hoshiya and Mandal 1984; Trautmann 1983; Paulin et al. 1998), N_h increases with $\tilde{u}$, reaches the peak value and then decreases to a residual value. For deeper conditions (e.g. $\widetilde{H}$ = 6 & 8), the decrease in N_h continues even at large $\tilde{u}$; however, for simplicity, the N_h after the square symbols is assumed to be constant (residual) for further discussion. Figure 6 also shows that, for a given $\widetilde{H}$ and B (= D), an anchor offers higher resistance than pipe. Note that, in a limited number of centrifuge tests, Dickin (1988) found higher residual resistance for an anchor than a similar-sized (B = D) pipe, although the peak resistances were similar. In other words, there is a "shape effect" on lateral resistance—the resistance is higher for the flat-surfaced anchor than the curve-surfaced pipe. In addition, $\tilde{u}$ required to mobilize the peak and residual resistances is higher for the anchor than for the pipe (e.g. $\tilde{u}$ at A′ is greater than $\tilde{u}$ at A, Fig. 6). This is because of the difference in soil failure mechanisms between anchors and pipes, as will be discussed in the following sections.

FE analyses are also performed for a large $\widetilde{H}$ (= 15). No significant increase in peak resistance occurs for an increase in $\widetilde{H}$ from 8 to 15. Moreover, the post-peak degradation of resistance for $\widetilde{H}$ = 15 is not significant.

Failure Mechanisms

The trend of lateral resistance shown in the previous sections can be further explained from the progressive development of shear bands (Figs. 7(a)–(x)). For small embedment ratios ($\widetilde{H}$= 2–4), the lateral displacement of the pipe or anchor results in formation of active and passive soil wedges, which is known as "wedge" type failure (Figs. 7 (a–l)). For a pipe at $\widetilde{H}$ = 2, γ^p accumulates mainly in three shear bands, and the length of the shear bands increases with lateral displacement of the pipe (Figs. 7(a–c)). At the peak, γ^p generates in the shear bands mainly near the pipe, while γ^p is very small when it is far from the pipe. This implies that, in the segments of the shear band far from the pipe, γ^p is not sufficient to mobilize the peak friction and dilation angles. Figure 7(b) shows that significant γ^p generates in the shear band which reduces ϕ' and ψ of the soil elements in the shear bands. At large displacements, the accumulation of γ^p in the shear bands continues together with a significant movement of the wedges resulting in ground heave above the passive wedge and settlement above the active wedge. A very similar pattern of failure planes and ground movement has been reported from physical model tests (Paulin et al. 1998; O'Rourke et al. 2008; Burnett 2015; Monroy et al. 2015).

Similar to the pipe case, three shear bands develop progressively for an anchor (Figs. 7(d–f)). At the peak, γ^p in the shear band is higher for the anchor than for the pipe (Figs. 7(a) and 7(d)). Moreover, a larger passive wedge forms for the anchor than for the pipe (compare Fig. 7(b) and 7(e)). The distance between the center of the anchor and the point where f_1 reaches the ground surface (l_a) is ~ 4.5B, while for the pipe, this distance (l_p) is ~ 4D. Because of this larger size of the passive wedge ($l_a > l_p$), the anchor offers higher resistance than pipe, as shown in Fig. 6. A similar response is found for $\widetilde{H}$ = 4 (Figs. 7(g–l)); however, $l_a/l_p \sim 1.3$ (as compared to $l_a/l_p \sim 1.1$ for $\widetilde{H}$ = 2), which is the primary reason for a significant difference between the resistances for pipe and anchor for $\widetilde{H}$ = 4 (Fig. 6). Dickin and Leung (1985) observed the formation of similar failure planes in their centrifuge tests for $\widetilde{H}$ = 2.5 and 4.5.

For a moderate embedment ratio ($\widetilde{H}$ = 6 & 8), at the peak, plastic deformation occurs mainly around the pipe (Fig. 7(m)). However, for the anchor, two horizontal shear bands in the front and a curved shear band at the back form at this stage (Fig. 7(p)). Three distinct shear bands, similar to the small embedment ratio cases, form at relatively large $\tilde{u}$ (Figs. 7(n) & 7(q)). At large $\tilde{u}$, a number of shear bands also form around the pipe and anchor, which also influence the force–

displacement behaviour. Not shown in Fig. 7, at large burial depths ($\widetilde{H}$ = 15), only local flow around mechanisms are observed both for anchor and pipe.

In summary, the force–displacement curves obtained from the model tests or numerical analysis evolve from complex soil failure mechanisms during lateral loading. Because of the considerable difference in soil failure mechanisms, anchors offer higher resistance than pipes.

Proposed simplified equations

A set of simplified equations is proposed in this section to calculate the peak (N_{hp}) and residual (N_{hr}) resistances for pipes and anchors. These equations are developed based on the following trend observed in model tests and the present FE simulations: (i) both N_{hp} and N_{hr} increase with $\widetilde{H}$; however, N_{hp} remains constant after a critical embedment ratio ($\widetilde{H}_c$); (ii) the difference between N_{hp} and N_{hr} is not significant at large $\widetilde{H}$; (iii) for a given $\widetilde{H}$, the smaller the pipe diameter or anchor height, the higher the N_{hp} and N_{hr}; (iv) for a given $B = D$, anchor resistance is higher than pipe resistance.

In order to capture these phenomena, the following equations are proposed:

(11) $N_{\mathrm{hp}} = N_{\mathrm{hp0}}\widetilde{H}^{\mathrm{m_p}} f_{\mathrm{D}} f_{\mathrm{s}}$ for $\widetilde{H} \leq \widetilde{H}_{\mathrm{c}}$

(12) $N_{\mathrm{hp}} = N_{\mathrm{hp0}}\widetilde{H}_{\mathrm{c}}^{\mathrm{m_p}} f_{\mathrm{D}} f_{\mathrm{s}}$ for $\widetilde{H} > \widetilde{H}_{\mathrm{c}}$

(13) $N_{\mathrm{hr}} = N_{\mathrm{hr0}}\widetilde{H}^{\mathrm{m_r}} f_{\mathrm{D}} f_{\mathrm{s}}$ with $N_{\mathrm{hr}} \leq N_{\mathrm{hp}}$

where N_{hp0} and N_{hr0} are the values of N_{hp} and N_{hr}, respectively, for a reference diameter of the pipe (D_0) and embedment ratio ($\widetilde{H}_0$); f_D is a size factor (e.g. the effects of D/D_0 for pipes and B/B_0 for anchors); f_s is a shape factor (i.e. pipe or anchor); and m_p and m_r are two constants.

In the present study, D_0 = 500 mm and $\widetilde{H}_0$ = 1 are used. Guo and Stolle (2005) used their FE calculated resistance for a 330-mm diameter pipe buried at $\widetilde{H}$ = 2.85 as the reference value to estimate the peak resistance for other pipe diameters and embedment ratios. To provide a simplified equation for the reference resistance, the following equation proposed by O'Rourke and Liu (2012) for shallow-buried pipeline is used in the present study.

$$N_{\mathrm{hp0}} = \frac{(\widetilde{H} + 0.5)^2 \tan\left(45° + \frac{\phi'_e}{2}\right)(\sin\beta + \mu_1 \cos\beta)}{2\widetilde{H}(\cos\beta - \mu_1 \sin\beta)} \quad (14)$$

where ϕ'_e is the equivalent friction angle, $\mu_1 = \tan\phi'_e$, and $\beta = 45° - \phi'_e/2$ is the inclination of an assumed linear slip plane to the horizontal that generates from the bottom of the pipe to form the passive wedge (i.e. an approximate linear line through the shear band f_1 in Fig. 3(d)).

When the peak resistance is mobilized, the plastic shear strain along the entire shear band is not the same—in some segments $\gamma^p < \gamma^p_p$ (i.e. pre-peak hardening state) while in some segments $\gamma^p > \gamma^p_p$ (i.e. post-peak softening state). Therefore, if one wants to use only one approximate value of ϕ' for the entire length of the shear band, (i.e. ϕ'_e in Eq. (14)), it should be less than ϕ'_p. Therefore, ϕ'_e = 44° is used in Eq. (14) to calculate N_{hp0}. Note that a similar approach of using ϕ'_e to calculate the bearing capacity of footing on dense sand, where shear bands form progressively, has been presented by Loukidis and Salgado (2011). Similarly, a representative value of ϕ' ($<\phi'_p$) has also been used to calculate the anchor resistance (Dickin and Leung 1983; Dickin 1994).

To calculate N_{hr0}, $\mu_1 = \tan\phi'_c$ is used, because, at this stage, significant plastic shear strains generate along the entire length of the failure plane that reduce ϕ' to the critical state value (e.g. Fig. 7(b)). It is also found that β does not change significantly with lateral displacement (e.g. see Figs. 7(a–c)). Therefore, β is calculated using ϕ'_e = 44°.

Similar to the work of Guo and Stolle (2005), the size factor is calculated using $f_D = 0.91(1 + D_0/(10D))$. The present FE results also show that $\widetilde{H}_c$ is higher for smaller size pipes or anchors, which is incorporated using $\widetilde{H}_c = f_{Hc}\widetilde{H}_{c0}$, where $f_{Hc} = 0.6(1 + D_0/(1.5D))$.

For the geometry and soil properties used in the present study, the peak resistance remains constant after $\widetilde{H} \sim 7.5$ for a 500-mm diameter pipe. Therefore, $\widetilde{H}_{c0} = 7.5$ is used for the reference condition. It is also found that the calculated resistances using Eqs. (11) to (13) fit well with the FE results for $m_p = 0.37$ and $m_r = 0.5$. Note that, Guo and Stolle (2005) found $m_p = 0.35$ as the representative value from their FE analysis. FE analyses also show that, for a given $B = D$, the anchor resistance is ~ 10% higher than pipe resistance (i.e. $f_s = 1.0$ for pipes and $f_s = 1.1$ for anchors).

Figure 8(a) shows that N_{hp} and N_{hr} obtained from Eqs. (11) to (13) match well with FE calculated values. The considerable difference between N_{hp} for different pipe dimeters is similar to that in the work of Guo and Stolle (2005). For a large embedment ratio (e.g. $\widetilde{H} > 10$ for $D = 500$ mm), $N_{hp} = N_{hr}$. Physical model tests on dense sand also show no significant reduction of post-peak reduction of resistance at large $\widetilde{H}$ (Hsu 1993).

Figure 8(b) shows that, when $f_s = 1.1$ is used for the anchor, Eqs. (11) to (13) calculate N_{hp} and N_{hr} similar to FE results. A significant difference in N_{hp} between small and large sized anchors at large $\widetilde{H}$ was also found in physical model tests, as shown in Fig. 5. In order to show the importance of the shape factor f_s, N_{hp} for the reference pipe ($D_0 = 500$ mm) is also shown in this figure, which is below the FE calculated values for a 500-mm high anchor.

In summary, while Guo and Stolle (2005) found a gradual increase in N_{hp} for pipe with the embedment ratio, the present study shows that both N_{hp} and N_{hr} increase with $\widetilde{H}$ for pipes and anchors, and reach a constant maximum value after a large $\widetilde{H}$. For practical purposes, without conducting FE analysis, the reference resistance can be calculated using the O'Rourke and Liu (2012) analytical solution with an equivalent friction angle (Eq. (14)). The present FE analysis and the simplified equations provide a method to estimate the peak and residual resistances. Finally, the above calculations are valid only for the given reference conditions ($D = 500$ mm and $\widetilde{H} = 1$);

for other reference conditions at shallow burial depths ($\widetilde{H}_0 < 3.0$), the model parameters in Eqs. (11)–(13) and ϕ'_e in Eq. (14) might be different.

Conclusions

Under lateral loading, the behaviour of buried pipelines and vertical strip anchors are generally assumed to be similar. In the present study, the similarities and differences between the behaviour of pipes and vertical strip anchors in dense sand subjected to lateral loading are examined through a comprehensive FE analysis. A modified Mohr-Coulomb (MMC) model for dense sand that captures the variation of friction and dilation angles with plastic shear strain, confining pressure and relative density are implemented in the FE analysis. The plastic shear strain localization (shear band) is successfully simulated, which can explain the soil failure mechanisms and the variation in lateral resistance for pipes and anchors for a wide range of embedment ratios. The proposed MMC model can simulate the peak resistance and also the post-peak degradation, as observed in physical model tests, which cannot be done using the Mohr-Coulomb model. The following conclusions can be drawn from the present study:

- The peak and residual resistances (N_{hp} and N_{hr}) increase with the embedment ratio ($\widetilde{H}$) both for pipes and anchors. However, after a critical $\widetilde{H}$, N_{hp} remains almost constant. The anchor resistance is ~ 10% higher than that of a similar-sized pipe.
- The critical embedment ratio ($\widetilde{H}_c$) is higher for smaller diameter pipe.
- The difference between N_{hp} and N_{hr} is significant at small to moderate $\widetilde{H}$; however, the difference is not significant at large $\widetilde{H}$.
- Both N_{hp} and N_{hr} are higher for smaller diameter pipes and smaller height of anchors.
- At a small $\widetilde{H}$, the soil failure mechanisms involve dislocation of active and passive wedges bounded by three distinct shear bands. At an intermediate $\widetilde{H}$, the active and passive wedges

form at large displacements of the anchor/pipe. However, at a large $\widetilde{H}$, flow around mechanisms govern the behaviour.

- The transition from shallow to deep failure mechanisms occurs at a lower $\widetilde{H}$ in pipes than in anchors.
- The mobilized ϕ' along the entire length of the shear band at the peak or post-peak degradation stages is not constant, because it depends on plastic shear strain. Even when N_{hp} is mobilized, $\phi' = \phi'_p$ only in a small segment of the shear band. Therefore, an equivalent friction angle, ϕ'_e ($< \phi'_p$) is required to match the peak resistance in test results. At a very large displacement, ϕ' in the shear bands ~ ϕ'_c because of significant strain accumulation in these zones.
- The proposed simplified equations can be used to estimate the peak and residual resistances of pipelines and anchors for shallow to intermediate embedment ratios. For large burial depths, no significant difference between these two resistances is found.

One practical implication of the present numerical study is that the parametric study can complement existing experimental data because it covers a wide range of pipe diameters and burial depths, including the cases of large diameter pipes and large embedment ratios, which represent the conditions of very costly full-scale tests. A limitation of this study is related to the selection of soil parameters for the MMC model. Additional laboratory tests in plane strain condition are required for a better estimation of model parameters to define the variation of mobilized friction and dilation angles.

Acknowledgements

The work presented in this paper was supported by the Research and Development Corporation of Newfoundland and Labrador, Chevron Canada Limited and the Natural Sciences and Engineering Research Council of Canada (NSERC).

List of symbols

The following abbreviations and symbols are used in this paper:

TX	triaxial
PS	plane strain
FE	finite element
PIV	particle image velocimetry
MC	Mohr–Coulomb model
MMC	modified Mohr–Coulomb model
A_ψ	slope of $(\phi'_p - \phi'_c)$ vs. I_R curve, Eq. (2)
m, C_1, C_2	soil parameters, Eqs. (4) and (5)
D_r	relative density
B	height of the strip anchor
D	diameter of pipe
D_0	reference diameter of pipe
E	Young's modulus
F_h	lateral force
H	distance from ground surface to the center of pipe/anchor
$\widetilde{H}$	embedment ratio
$\widetilde{H}_0$	reference embedment ratio
$\widetilde{H}_c$	critical embedment ratio
$\widetilde{H}_{c0}$	reference critical embedment ratio
I_R	relative density index
K	material constant
K_0	at-rest earth pressure coefficient
N_h	normalized lateral resistance

N_{hp}, N_{hr} normalized peak and residual resistances

N_{hp0}, N_{hr0} reference peak and residual resistances

Q, R material constants (Bolton 1986)

d_{50} mean particle size

f shear bands

f_{HC} size factor for critical embedment ratio

f_D size factor for normalized resistance

f_s shape factor

k_ψ slope of $(\phi'_p - \phi'_c)$ vs. ψ_p curve, Eq. (3)

l_a, l_p width of passive failure wedges, Fig.7

m_p, m_r constants in Eqs. (12) and (13)

n an exponent in Eq. (10)

p' mean effective stress

t_s thickness of shear band

t_{FE_ref} reference FE mesh size

t_{FE} FE mesh size

u lateral displacement of pipe/anchor

$\tilde{u}$ normalized lateral displacement

β inclination of linear slip plane to the horizontal

μ interface friction coefficient

$\dot{\epsilon}^p_{ij}$ plastic deviatoric strain rate

ϕ' mobilized angle of internal friction

ϕ'_{in} ϕ' at the start of plastic deformation

ϕ'_p peak friction angle

ϕ'_c critical state friction angle

ϕ'_e equivalent friction angle

ϕ_μ pipe/anchor–soil interface friction angle

ψ mobilized dilation angle

ψ_p peak dilation angle

γ unit weight of soil

γ^p engineering plastic shear strain

γ^p_p γ^p required to mobilize ϕ'_p

γ^p_c strain softening parameter

References

Akinmusuru, J.O. 1978. Horizontally loaded vertical anchor plates in sand. Journal of the Geotechnical Engineering Division, **104**(2): 283–286.

American Lifelines Alliance (ALA). 2005. Guidelines for the design of buried steel pipe. Available from https://www.americanlifelinesalliance.com/pdf/Update061305.pdf [accessed 13 March 2017].

Anastasopoulos, I., Gazetas, G., Bransby, M.F., Davies, A., and El Nahas, M.C.R. 2007. Fault rupture propagation through sand: finite-element analysis and validation through centrifuge experiments. Journal of Geotechnical and Geoenvironmental Engineering, **133**(8): 943–958.

Andresen, L. and Jostad, H.P. 2004. Analyses of progressive failure in long natural slopes. *In* Proceedings of the 9th International Symposium on Numerical Models in Geotechnics, Ottawa, Canada, pp. 603–608.

Audibert, J.M.E., and Nyman, K.J. 1978. Soil restraint against horizontal motion of pipes. International Journal of Rock Mechanics and Mining Sciences, **15**(2): A29.

Bhattacharya, P. and Kumar, J. 2013. Seismic pullout capacity of vertical anchors in sand. Geomechanics and Geoengineering, **8**(3): 191–201.

Bishop, A.W. 1961. Discussion on soil properties and their measurement. *In* Proceedings of the 5th International Conference on Soil mechanics and Foundation Engineering, p. 3.

Bolton, M.D. 1986. The strength and dilatancy of sands. Géotechnique, **36**(1): 65−78.

Burnett, A. 2015. Investigation of full scale horizontal pipe−soil interaction and large strain behaviour of sand. M.A.Sc. thesis, Queen's University, Canada.

Chakraborty, T., and Salgado, R. 2010. Dilatancy and shear strength of sand at low confining pressures. Journal of Geotechnical and Geoenvironmental Engineering, **136**(3): 527–532.

Choudhary, A.K. and Dash, S.K. 2017. Load carrying mechanism of vertical plate anchors in sand. International Journal of Geomechanics, **17**(5): 04016116.

Clukey, E.C., Haustermans, L. and Dyvik, R. 2005. Model tests to simulate riser−soil interaction effects in touchdown point region. *In* Proceedings of the International Symposium on Frontiers in Offshore Geotechnics (ISFOG 2005), Perth, Australia, pp. 651−658.

Cornforth, D.H. 1964. Some experiments on the influence of strain conditions on the strength of sand. Géotechnique, **14**:143−167.

Daiyan, N., Kenny, S., Phillips, R., and Popescu, R. 2011. Investigating pipeline–soil interaction under axial–lateral relative movements in sand. Canadian Geotechnical Journal, **48**(11): 1683−1695.

Dassault Systèmes. 2010. ABAQUS [computer program]. Dassault Systèmes, Inc., providence, R.I.

Das, B.M., Seeley, G.R., and Das, S.C. 1977. Ultimate resistance of deep vertical anchor in sand. Soils and Foundations, **17**(2): 52–56.

Das, B.M. and Shukla, S.K. 2013. Earth Anchors. 2nd edition, J. Ross Publishing Inc, USA.

Debnath, P. 2016. Centrifuge modeling of oblique pipe–soil interaction in dense and loose sand. M.Eng. thesis, Memorial University of Newfoundland, Canada.

Dickin, E.A. 1988. Stress–displacement of buried plates and pipes. *In* Proceedings of the International Conference on Geotechnical Centrifuge Modelling, Centrifuge 88, Paris, France.

Dickin, E.A. 1994. Uplift resistance of buried pipelines in sand. Soils and Foundations, **34**(2): 41–48.

Dickin, E.A. and Laman, M. 2007. Uplift response of strip anchors in cohesionless soil. Advances in Engineering Software, **38**: 618–625.

Dickin, E.A., and Leung, C.F. 1983. Centrifuge model tests on vertical anchor plates. Journal of Geotechnical Engineering, **12**(1503): 1503–1525.

Dickin, E.A., and Leung, C.F. 1985. Evaluation of design methods for vertical anchor plates. Journal of Geotechnical Engineering, **4**(500): 500–520.

Dickin, E.A. and King, G.J.W. 1993. Finite element modelling of vertical anchor walls in sand. *In* Proceedings of the Developments in Civil & Construction Engineering Computing, Civil-Comp Press, Edinburgh, UK.

Duncan, J.M., and Chang, C.Y. 1970. Nonlinear analysis of stress and strain in soils. J. Soil Mech. Found. Div., **96**(5): 1629–1653.

Guo, P. 2012. Critical length of force chains and shear band thickness in dense granular materials. Acta Geotechnica, **7**: 41–55.

Guo, P., and Stolle, D. 2005. Lateral pipe–soil interaction in sand with reference to scale effect. Journal of Geotechnical and Geoenvironmental Engineering, **131**(3): 338–349.

Hansen, J.B. and Christensen, N.H. 1961. The ultimate resistance of rigid piles against transversal forces. Bulletin 12, Danish Geotechnical Institute, Copenhagen, Denmark.

Hardin, B.O., and Black, W.L. 1966. Sand stiffness under various triaxial stress. Journal of the Soil Mechanics and Foundation Engineering, ASCE, **92**(SM2): 27−42.

Houlsby, G.T. 1991. How the dilatancy of soils affects their behaviour. *In* Proceedings of the 10th European Conference on Soil Mechanics and Foundation Engineering, Florence, pp. 1189–1202.

Hoshiya, M. and Mandal, J.N. 1984. Some studies of anchor plates in sand. Soils and Foundations, **24**(1): 9–16.

Hsu, T. 1993. Rate effect on lateral soil restraint of pipelines. Soils and Foundations, **33**(4): 159−169.

Janbu, N. 1963. Soil compressibility as determined by oedometer and triaxial tests. *In* Proceedings of the European Conference on Soil Mechanics and Foundation Engineering, Wiesbaden, Germany, pp. 19−25.

Jefferies, M., and Been, K. 2006. Soil liquefaction: a critical state approach. 2nd edition, Taylor & Francis, New York.

Jung, J.K., O'Rourke, T.D., and Olson, N.A. 2013. Lateral soil-pipe interaction in dry and partially saturated sand. Journal of Geotechnical and Geoenvironmental Engineering, **139**(12): 2028–2036.

Jung, J.K., O′Rourke, T.D., and Argyrou, C. 2016. Multi-directional force–displacement response of underground pipe in sand. Canadian Geotechnical Journal, **53**(11): 1763–1781.

Kouretzis, G.P., Sheng, D., and Sloan, S.W. 2013. Sand–pipeline–trench lateral interaction effects for shallow buried pipelines. Computers and Geotechnics, **54**: 53–59.

Kumar, J., and Sahoo, J.P. 2012. An upper bound solution for pullout capacity of vertical anchors in sand using finite elements and limit analysis. International Journal of Geomechanics, **12**(3): 333–337.

Loukidis, D. and Salgado, R. 2008. Analysis of the shaft resistance of non−displacement piles in sand. Géotechnique, **58**(4): 283–296.

Loukidis, D. and Salgado, R. 2011. Effect of relative density and stress level on the bearing capacity of footings on sand. Géotechnique, **61**(2): 107–119.

Merifield, R.S. and Sloan, S.W. 2006. The ultimate pullout capacity of anchors in frictional soils. Canadian Geotechnical Journal, **43**(8): 852–868.

Monroy, M., Wijewickreme, D., Nyman, D.J. and Honegger, D.G. 2015. Soil restraint on steel buried pipelines under reverse fault displacement. *In* Proceedings of the 6th International Conference on Earthquake Geotechnical Engineering, Christchurch, New Zealand.

Moore, I.D. and Rowe, R.K. 1990. Scaling rule for localized plasticity in strain-softening continua. *In* Proceedings of the 1st International Conference on Computer Aided Assessment of Localized Damage, Portsmouth, pp. 99–112.

Murray, E.J., and Geddes, J.D. 1989. Resistance of passive inclined anchors in cohesionless medium. Géotechnique, **39**(3): 417–431.

Neely, W.J., Stewart, J.G., and Graham, J. 1973. Failure loads of vertical anchor plates in sand. Journal of the Geotechnical Engineering Division, ASCE, **99**(9): 669–685.

Ng, P.C.F. 1994. Behaviour of buried pipelines subjected to external loading. PhD thesis, University of Sheffield, UK.

O’Rourke, T.D. 2010. Geohazards and large, geographically distributed systems. Rankine lecture. Géotechnique, **60**(7): 505–543.

O'Rourke, M.J., and Liu, X. 2012. Seismic design of buried and offshore pipelines. MCEER Monograph, MCEER-12-MN04.

O'Rourke, T.D., Jezerski, J.M., Olson, N.A., and Bonneau, A.L. 2008. Geotechnics of pipeline system response to earthquakes. *In* Proceedings of the 4^{th} Decennial Geotechnical Earthquake Engineering and Soil Dynamics Conference (GEESD IV), ASCE, Sacramento, California.

Oswell, J.M. 2016. Soil Mechanics for Pipeline Stress Analysis. Naviq Consulting Inc.

Ovesen, N.K. and Stromann, H. 1972. Design methods for vertical anchor slabs in sand. *In* Proceedings of the Specialty Conference on Performance of Earth and Earth-Supported Structures, ASCE, **2**(1): 1481–1500.

Palmer, A.C., White, D.J., Baumgard, A.J., Bolton, M.D., Barefoot, A.J., Finch, M., Powell, T., Faranski, A.S., and Baldry, J.A.S. 2003. Uplift resistance of buried submarine pipelines: comparison between centrifuge modelling and full-scale tests. Géotechnique, **53**(10): 877−883.

Paulin, M.J., Phillips, R., Clark, J.I., Trigg, A. and Konuk, I. 1998. Full−scale investigation into pipeline/soil interaction. *In* Proceedings of the International Pipeline Conference (IPC), pp. 779−787.

Pietruszczak, St. and Mróz, Z. 1981. Finite element analysis of deformation of strain-softening materials. International Journal for Numerical Methods in Engineering, **17**: 327–334.

Pipeline Research Council International (PRCI). 2004. Guidelines for the seismic design and assessment of natural gas and liquid hydrocarbon pipelines, pipeline design, construction and operations. Edited by Honegger, D.G., and Nyman D.J.

Pradhan, T.B.S., Tatsuoka, F., and Horii, N. 1988. Strength and deformation characteristics of sand in torsional simple shear. Soils and Foundations, **28**(3): 131−148.

Robert, D.J., and Thusyanthan, N.I. 2014. Numerical and experimental study of uplift mobilization of buried pipelines in sands. Journal of Pipeline Systems Engineering and Practices, 6(1): 04014009.

Rowe, R.K. and Davis, E.H. 1982. Behaviour of anchor plates in sand. Géotechnique, **32**(1): 25−41.

Roy, K., Hawlader, B.C., Kenny, S. and Moore, I.D. 2016. Finite element modeling of lateral pipeline−soil interactions in dense sand. Canadian Geotechnical Journal, **53**(3): 490−504.

Roy, K., Hawlader, B.C., Kenny, S. and Moore, I.D. 2016(a). Finite element analysis of strip anchors buried in dense sand subjected to lateral loading. *In* Proceedings of 26th International Ocean and Polar Engineering Conference (ISOPE 2016), Rhodes, Greece, June 26–July 2, Paper # ISOPE-I-16-463.

Sakai, T., and Tanaka, T. 2007. Experimental and numerical study of uplift behavior of shallow circular anchor in two-layered sand. Journal of Geotechnical and Geoenvironmental Engineering, **133**(4): 469–477.

Sakai, T., Erizal, V., and Tanaka, T. 1998. Particle size effect of anchor problem with granular materials. *In* Proceedings of the 4th European Conference on Numerical Methods in Geotechnical Engineering, Udine, pp. 181–200.

Tagaya, K., Tanaka, A., and Aboshi, H. 1983. Application of finite element method to pullout resistance of buried anchor. Soils and Foundations, **23**(3): 91–104.

Tatsuoka, F., Okahara, M., Tanaka, T., Tani, K., Morimoto, T., and Siddiquee, M.S.A. 1991. Progressive failure and particle size effect in bearing capacity of a footing on sand. Geotechnical Special Publication, **27**(2): 788–802.

Tejchman, J. and Górski, J. 2008. Size effects in problems of footings on sand within micro-polar hypoplasticity. Archives of Hydro−engineering and Environmental Mechanics, **55**(3–3): 95–124.

Tejchman, J. and Herle, I. 1999. A “class A” prediction of the bearing capacity of plane strain footings on granular material. Soils and Foundations, **39**(5): 47–60.

Trautmann, C. 1983. Behavior of pipe in dry sand under lateral and uplift loading. PhD thesis, Cornell University, Ithaca, NY.

Trautmann, C.H. and O'Rourke, T.D. 1983. Load-displacement characteristics of a buried pipe affected by permanent earthquake ground movements. *In* Earthquake behaviour and safety of oil and gas storage facilities, buried pipelines and equipment. PVP-77. Edited by T. Ariman. American Society of Mechanical Engineers (ASME), New York. pp. 254–262.

Uesugi, M., Kishida, H., and Tsubakihara, Y. 1988. Behavior of sand particles in sand−steel friction. Soils and Foundations, **28**(1): 107–118.

White, D.J., Take, W.A., and Bolton, M.D. 2003. Soil deformation measurement using particle image velocimetry (PIV) and photogrammetry. Géotechnique, **53**(7): 619–631.

White, D.J., Cheuk, C.Y, and Bolton, M.D. 2008. The Uplift resistance of pipes and plate anchors buried in sand. Géotechnique, **58**(10): 771–779.

Yimsiri, S., Soga, K., Yoshizaki, K., Dasari, G., and O’Rourke, T. 2004. Lateral and upward soil−pipeline interactions in sand for deep embedment conditions. Journal of Geotechnical and Geoenvironmental Engineering, **130**(8): 830−842.

Yoshimine, M. 2005. Archives–soil mechanics laboratory. Tokyo Metropolitan University, Available from http://geot.civil.ues.tmu.ac.jp/archives/ [accessed 4 April 2015].

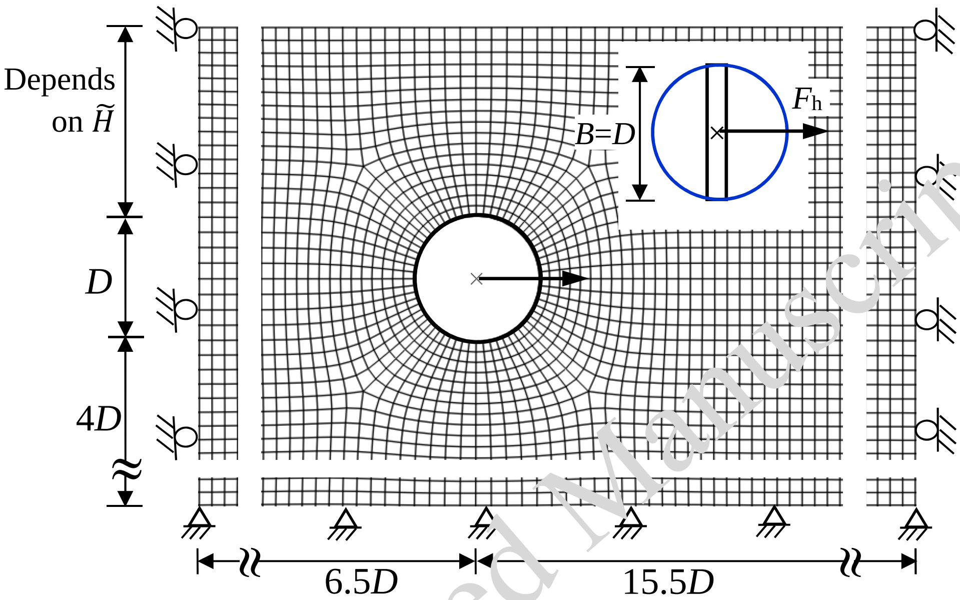

Fig. 1. Typical finite element mesh for D=500 mm

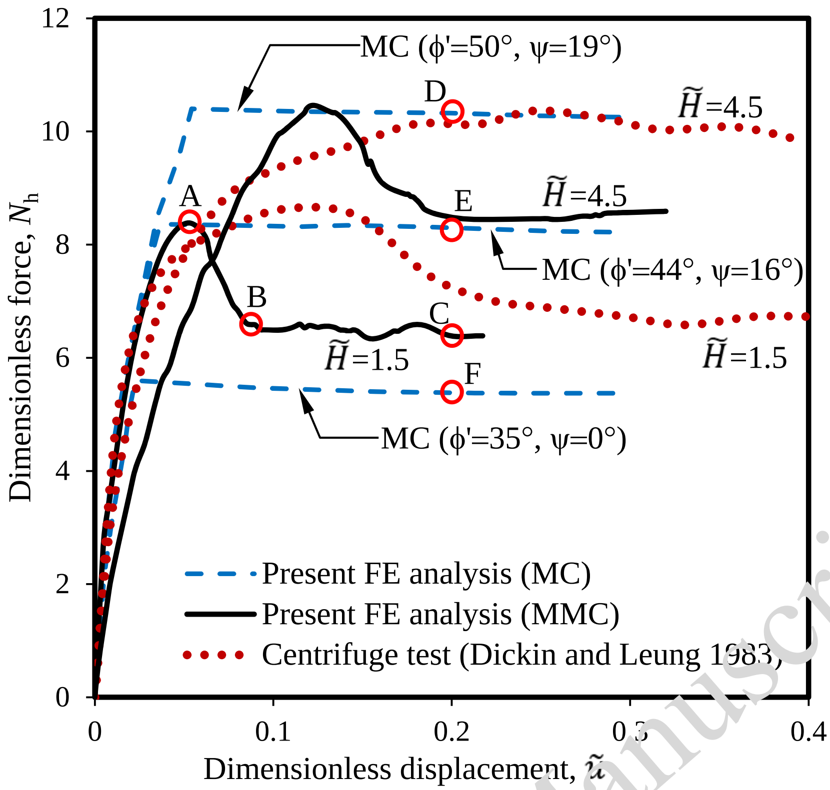

Fig. 2. Comparison between present FE analysis with physical model test results (a) anchor

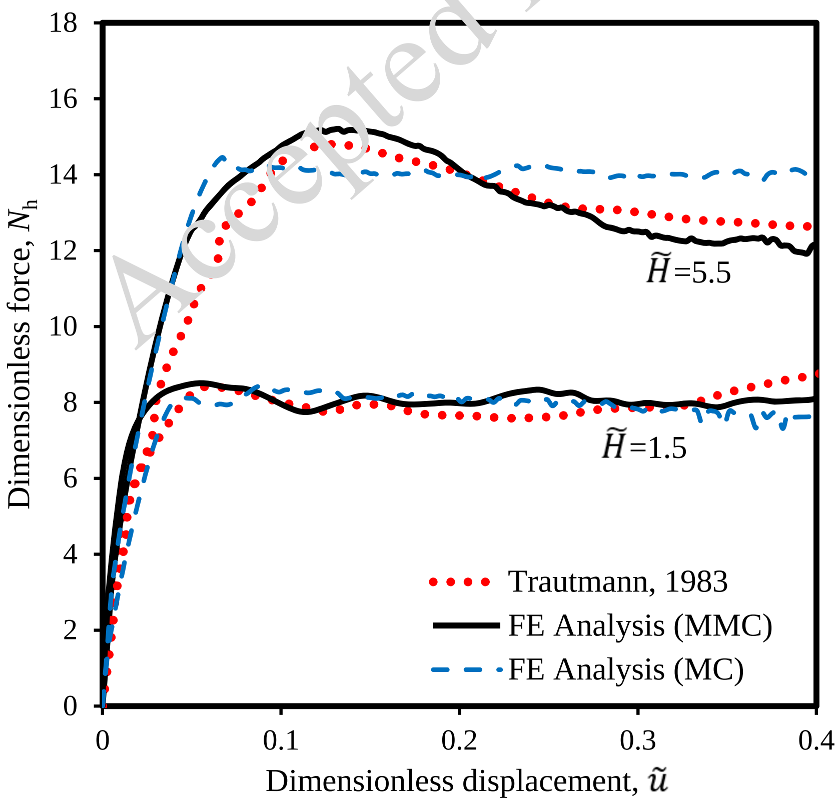

Fig. 2. Comparison between present FE analysis with physical model test results (b) pipe (Roy et al 2016)

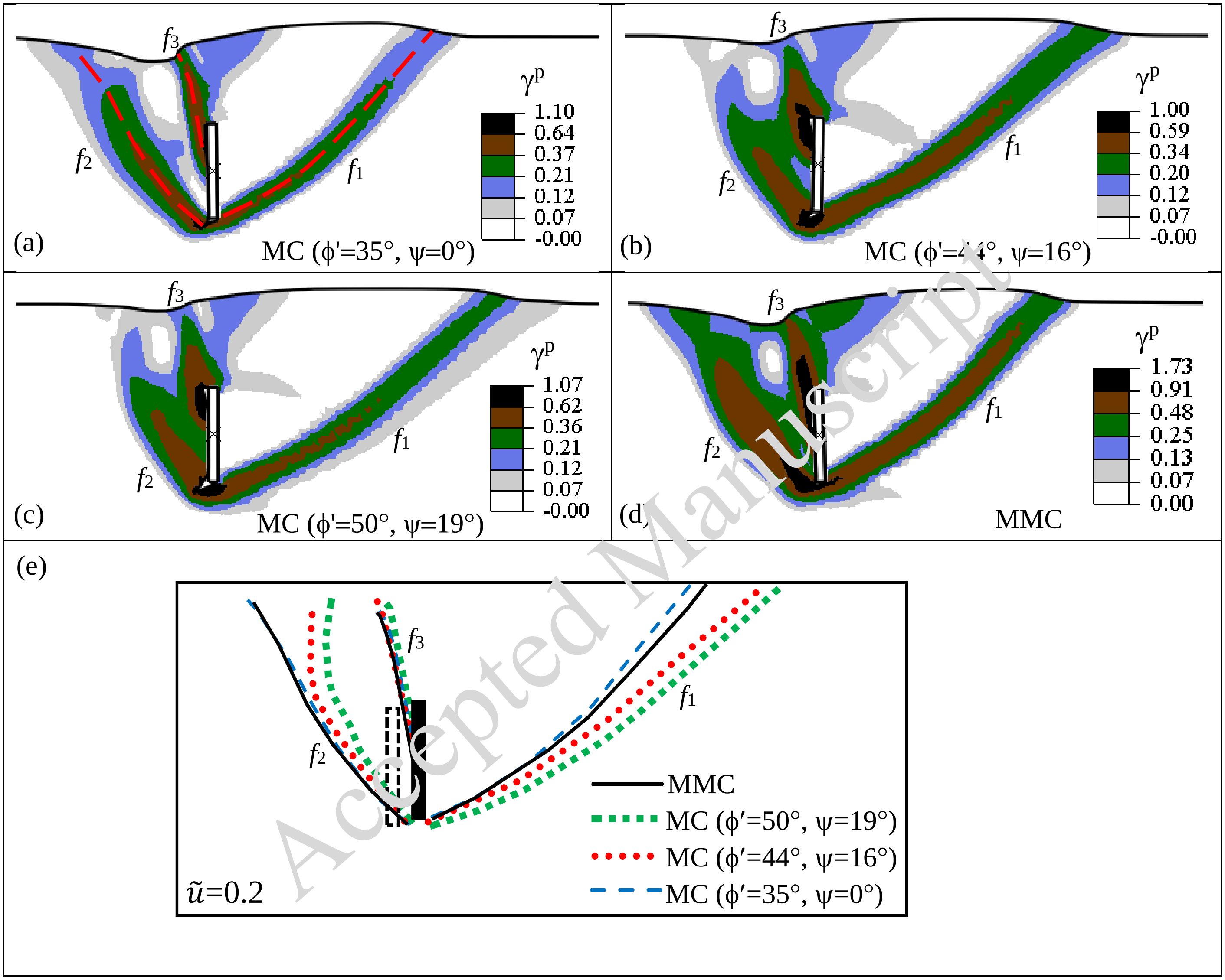

Fig. 3. Shear band formation for 1,000-mm high strip anchor with MC and MMC models

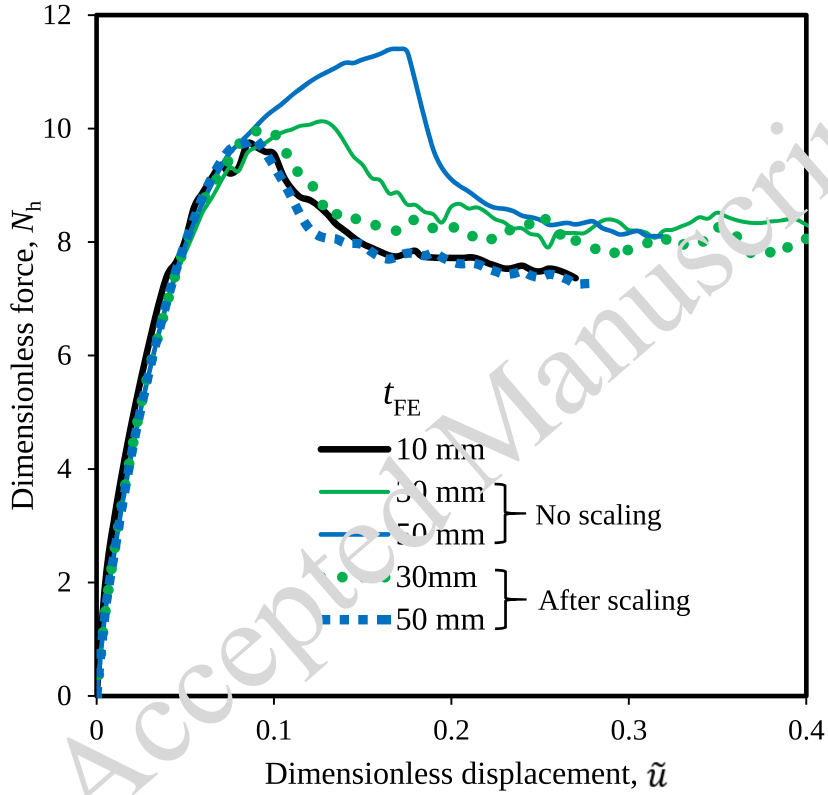

Fig. 4. Mesh sensitivity analysis for 500-mm diameter pipe with MMC model

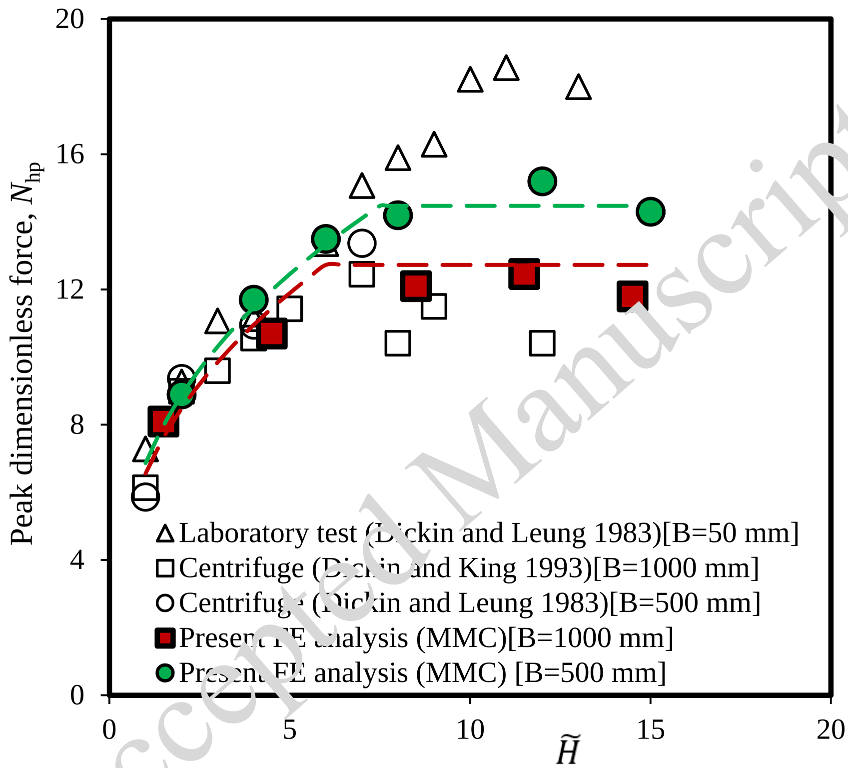

Fig. 5. Peak lateral resistance of anchors with burial depth

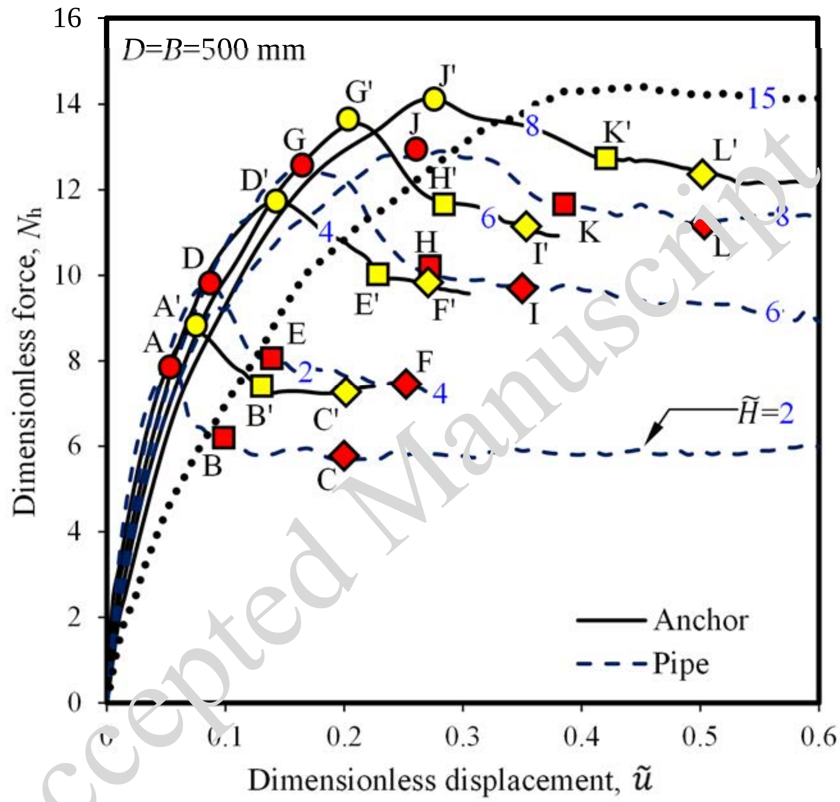

Fig. 6. Comparison between N_h–$\tilde{u}$ curves for pipes and strip anchors ($B = D = 500$ mm)

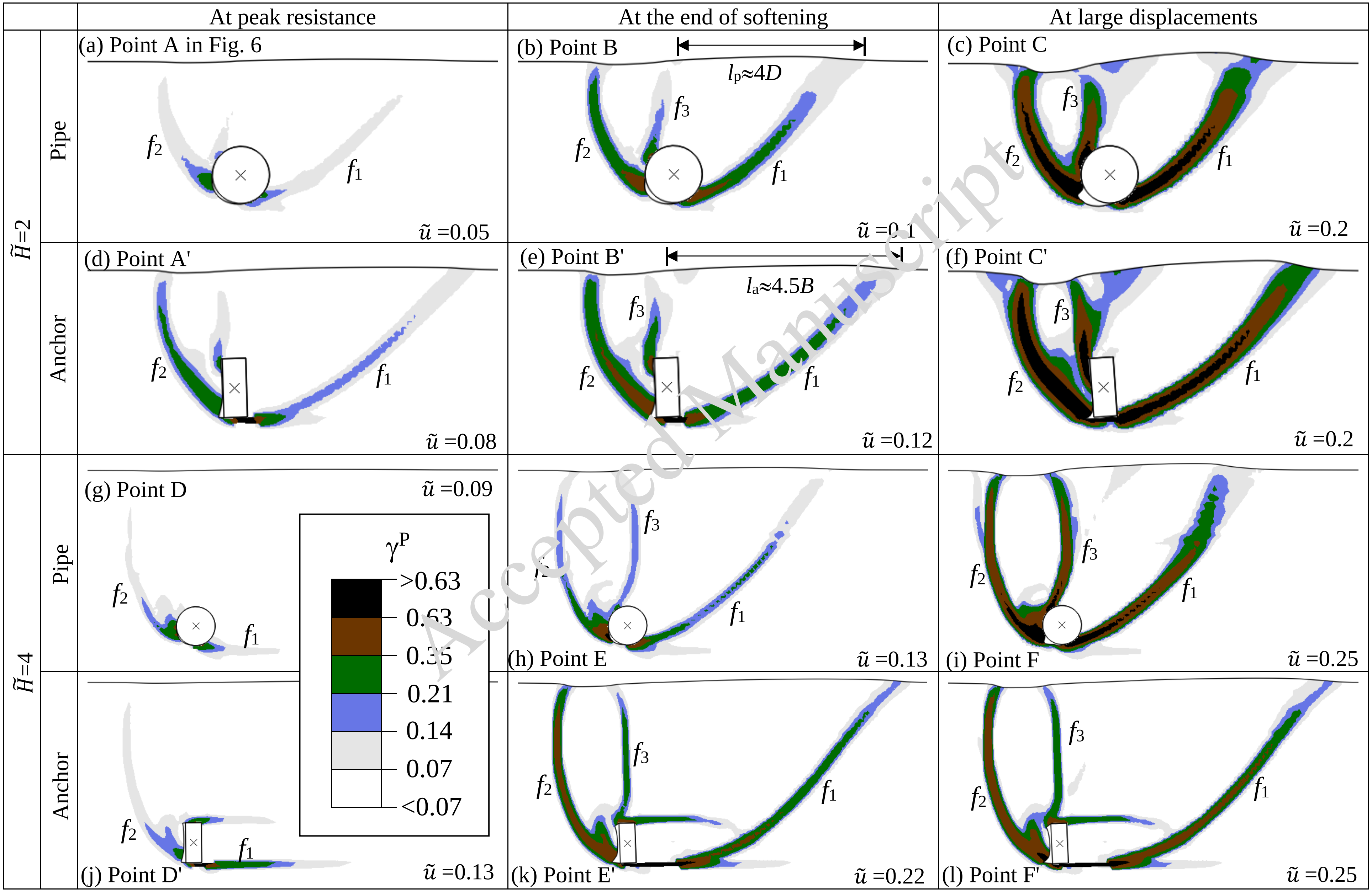
At peak resistance
At the end of softening
At large displacements
H̃=2
H̃=4
Pipe
Anchor
(a) Point A in Fig. 6
ũ =0.05
(b) Point B
l_p≈4D
ũ =0.1
(c) Point C
ũ =0.2
(d) Point A'
ũ =0.08
(e) Point B'
l_a≈4.5B
ũ =0.12
(f) Point C'
ũ =0.2
(g) Point D
ũ =0.09
(h) Point E
ũ =0.13
(i) Point F
ũ =0.25
(j) Point D'
ũ =0.13
(k) Point E'
ũ =0.22
(l) Point F'
ũ =0.25
f1
f2
f3
γ^P
>0.63
0.63
0.35
0.21
0.14
0.07
<0.07

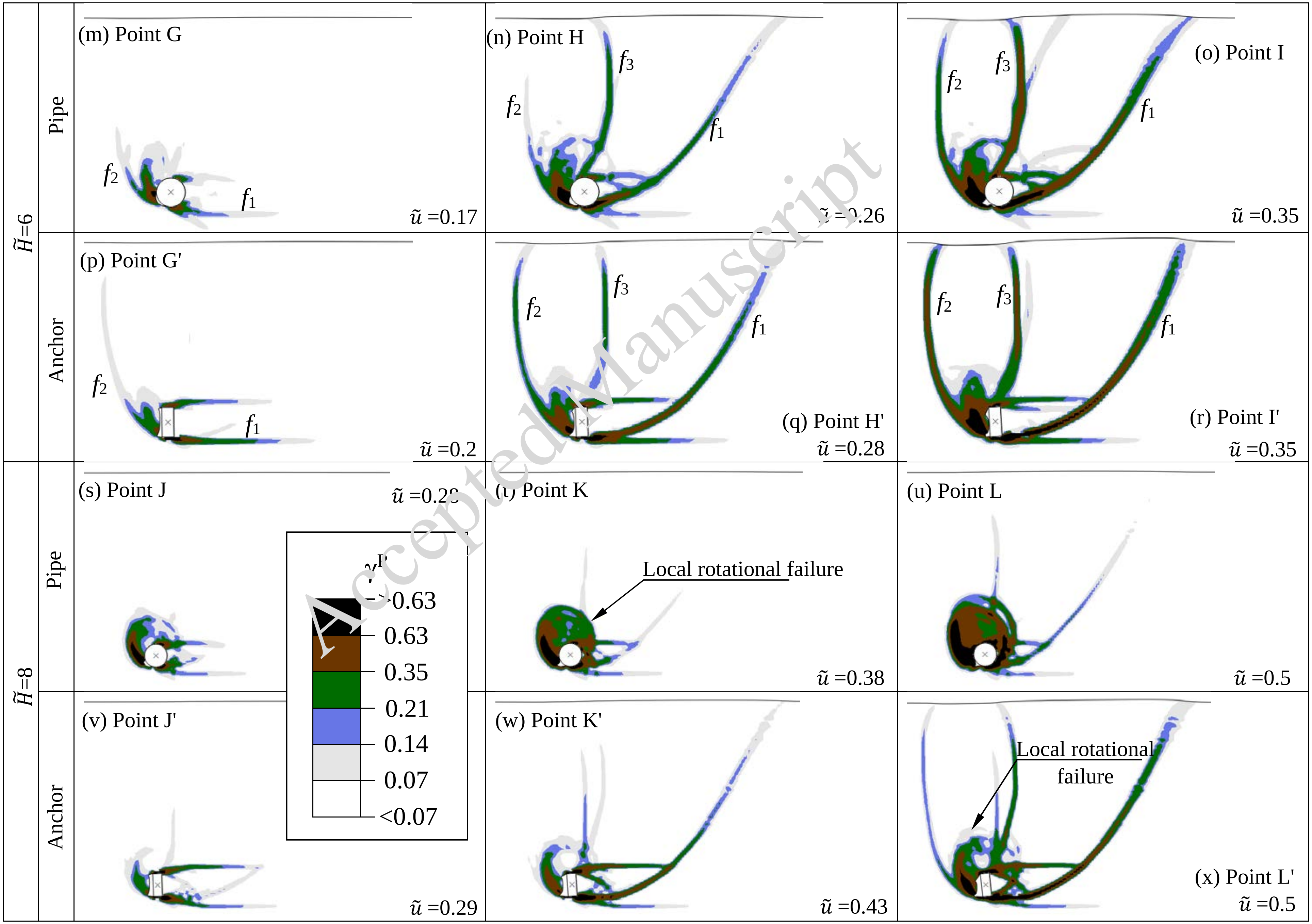

Fig. 7. Failure mechanism for 500-mm diameter pipe and 500-mm high anchor

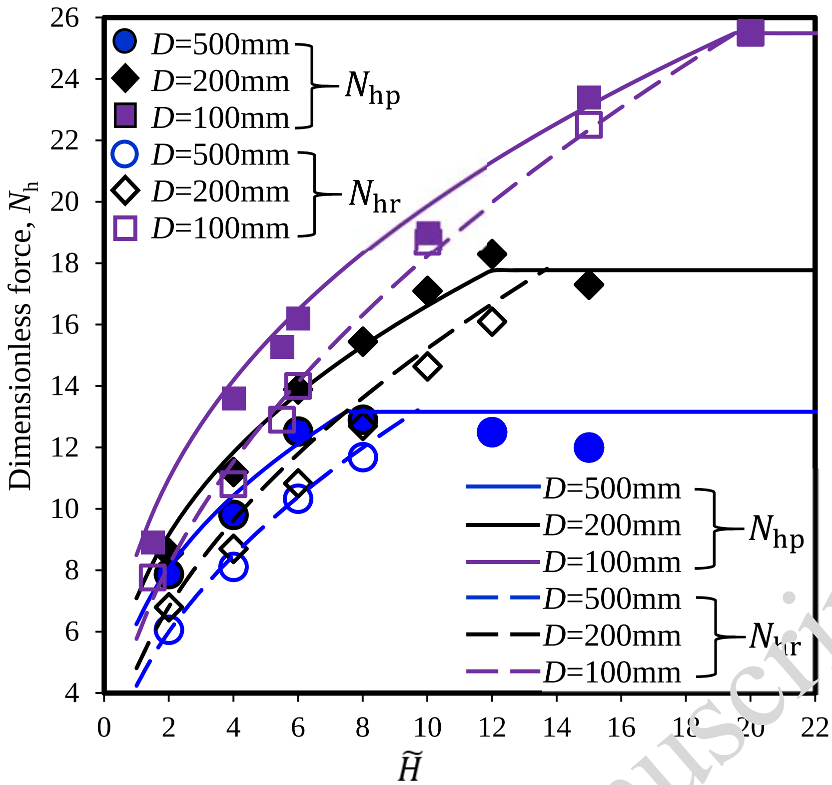

Fig. 8. Comparison between simplified equations and finite element results (a) for pipe

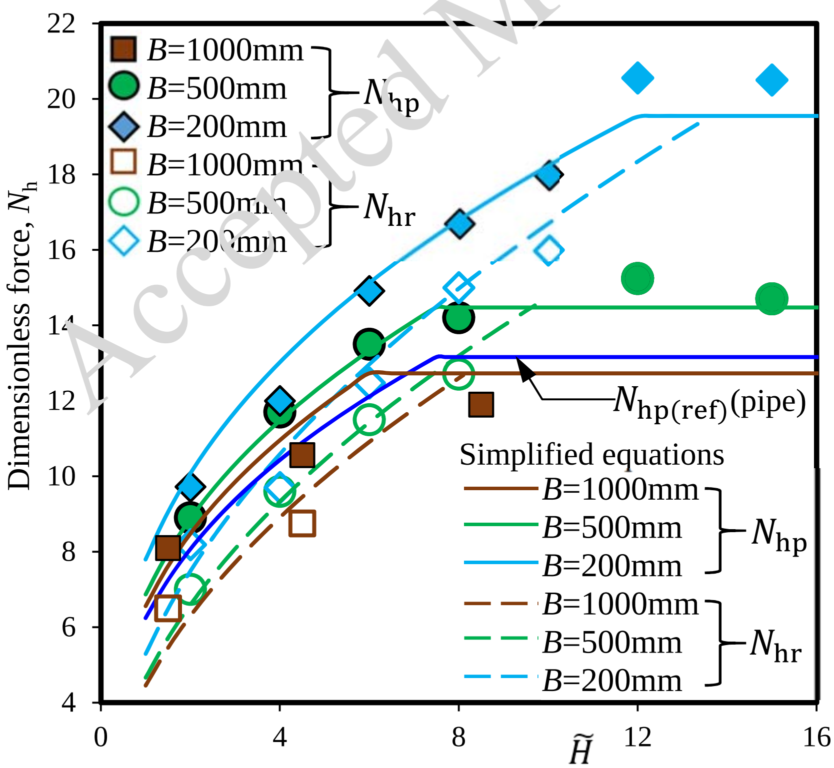

Fig. 8. Comparison between simplified equations and finite element results (b) for anchor

Table 1: Equations for Modified Mohr–Coulomb Model (MMC) (summarized from Roy et al. 2016)

Description	Eq. #	Constitutive Equations
Relative density index	(1)	$I_R = I_D(Q - \ln p') - R$ where $I_D = D_r(\%)/100$ & $0 \leq I_R \leq 4$
Peak friction angle	(2)	$\phi'_p - \phi'_c = A_\psi I_R$
Peak dilation angle	(3)	$\psi_p = \frac{\phi'_p - \phi'_c}{k_\psi}$
Strain-softening parameter	(4)	$\gamma^p_c = C_1 - C_2 I_D$
Plastic shear strain at ϕ'_p and ψ_p	(5)	$\gamma^p_p = \gamma^p_c \left(\frac{p'}{p'_a}\right)^m$
Mobilized friction angle in pre-peak stress–strain curve	(6)	$\phi' = \phi'_{in} + \sin^{-1}\left[\left(\frac{2\sqrt{\gamma^p \gamma^p_p}}{\gamma^p + \gamma^p_p}\right)\sin(\phi'_p - \phi'_{in})\right]$
Mobilized dilation angle in pre-peak stress–strain curve	(7)	$\psi = \sin^{-1}\left[\left(\frac{2\sqrt{\gamma^p \gamma^p_p}}{\gamma^p + \gamma^p_p}\right)\sin(\psi_p)\right]$
Mobilized friction angle in post-peak strain-softening region	(8)	$\phi' = \phi'_c + \left(\phi'_p - \phi'_c\right)\ \exp\left[-\left(\frac{\gamma^p - \gamma^p_p}{\gamma^p_c}\right)^2\right]$
Mobilized dilation angle in post-peak softening region	(9)	$\psi = \psi_p \exp\left[-\left(\frac{\gamma^p - \gamma^p_p}{\gamma^p_c}\right)^2\right]$
Young's modulus	(10)	$E = K p'_a \left(\frac{p'}{p'_a}\right)^n$

Table 2. Geometry and soil parameters used in the FE analyses

Parameter	Model test (Parametric Study)
External diameter of pipe, D (mm)	100 (200, 500)
Height of the strip anchor, B (mm)	1000 (200, 500)
Thickness of the strip anchor, t (mm)	200 (100)
K	150
n	0.5
Poisson's ratio of soil, ν_{soil}	0.2
A_{ψ}	5
k_{ψ}	0.8
ϕ'_{in} (°)	29
C_1	0.22
C_2	0.11
m	0.25
Critical state friction angle, ϕ'_c (°)	35
Relative density, D_r (%)	80
Unit weight of sand, γ (kN/m^3)	17.7*
Interface friction coefficient, μ	0.32
Embedment ratio, $\widetilde{H}$	1.5, 4.5, 5.5 (2, 4, 6, 8, 10, 12, 15)

Notes: *γ = 16 kN/m^3 is used for Dickin and Leung (1983) physical test simulations (Fig. 2(a)); numbers in parenthesis in right column show the values used in the parametric study